Supplemental Information

Bulk Properties of the Oxygen Reduction Catalyst SrCo$_{0.9}$Nb$_{0.1}$O$_{3-\delta}$

Robert E. Usiskin[1], Timothy C. Davenport[1], Richard Y. Wang[1], Webster Guan[2], Sossina M. Haile[1, 2*]

1. Materials Science, California Institute of Technology, Pasadena, CA, United States.

2. Chemical Engineering, California Institute of Technology, Pasadena, CA, United States.

*Corresponding author. Current address: Materials Science and Engineering, Northwestern University, Evanston, IL, United States. Email: sossina.haile@northwestern.edu

Table S1. R values for the Rietveld refinement shown in Figure 1.

Sample	R_{wp} (%)	R_p (%)	R_{wp} (-bkgd) (%)	R_p (-bkgd) (%)	χ^2
SCN as prepared	8.01	5.50	12.08	8.03	2.459
750 °C anneal for 4 d	6.31	4.75	7.00	5.46	1.524
750 °C anneal for 10 d	6.97	5.10	7.32	5.72	1.914
1200 °C anneal	7.46	5.25	10.35	7.00	2.068
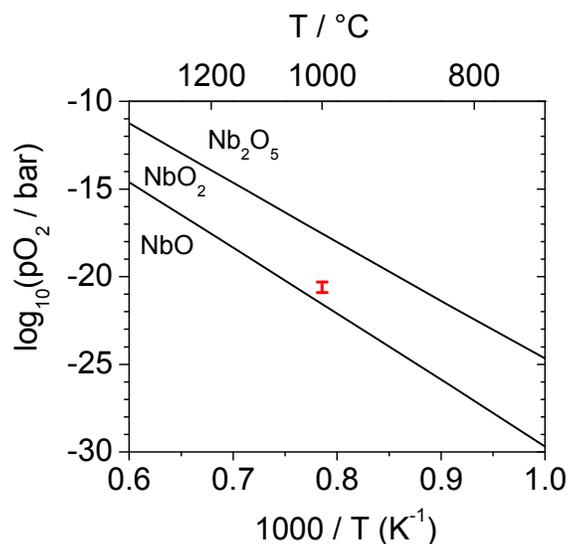
Figure S1. Thermodynamic stability limits in the Nb-O system, as calculated from Gibbs energies in the NIST-JANAF Thermochemical Tables [1985, version 1.0]. The red interval shown is the pO_2 range in the chamber during reduction, calculated based on the H_2 concentration (7.5%) and trace oxygen (50-100 ppm) entering into the system. These data indicate the reduction of Nb^{5+} to Nb^{4+} is expected under the reducing atmosphere utilized. (The oxygen partial pressure was not directly monitored in the case of extreme reduction due to concern of damage to the Pt electrodes in the oxygen sensor.)
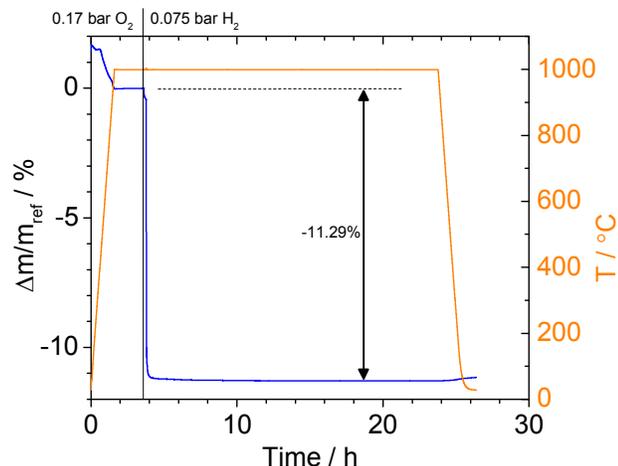
Figure S2. Buoyancy-corrected thermogravimetric profile obtained by equilibrating a powder sample of $SrCo_{0.9}Nb_{0.1}O_{3-\delta}$ at 1000 °C in a mixture of 0.17 bar O_2 in Ar (total pressure 1 bar, equilibrated mass = 397.13 mg) and then introducing a mixture of 0.075 bar H_2 in Ar. Immediate reduction is apparent. Slight reoxidation occurs during cooling even in this very reducing environment, consistent with the predictions of Figure S1.
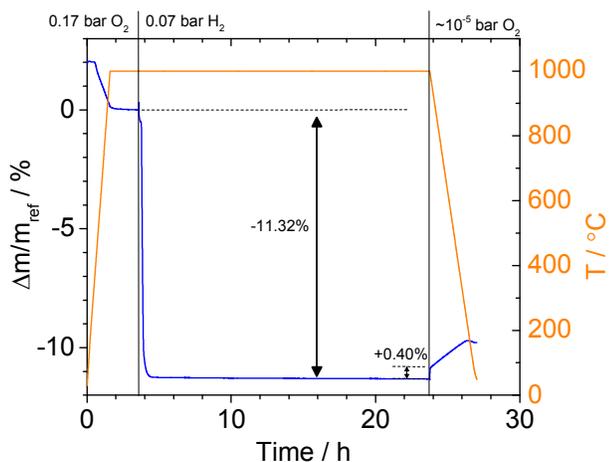
Figure S3. Repetition of the experiment in Figure S2 with a fresh sample, except here inert gas ($pO_2 \sim 10^{-5}$ bar) was introduced at the beginning of the final cooling step, whereupon an immediate 0.48% mass increase is seen, consistent with the oxygen mass uptake expected (0.46%) from the re-oxidation of Nb^{4+} to Nb^{5+} predicted by Figure S1. (A subsequent slower mass uptake is also observed and is attributed to slight uptake of water, *i.e.*, strontium hydroxide formation).

Based on Figures S1-S3, we conclude that only Nb^{4+} is present in the reduction products at 1000 °C.
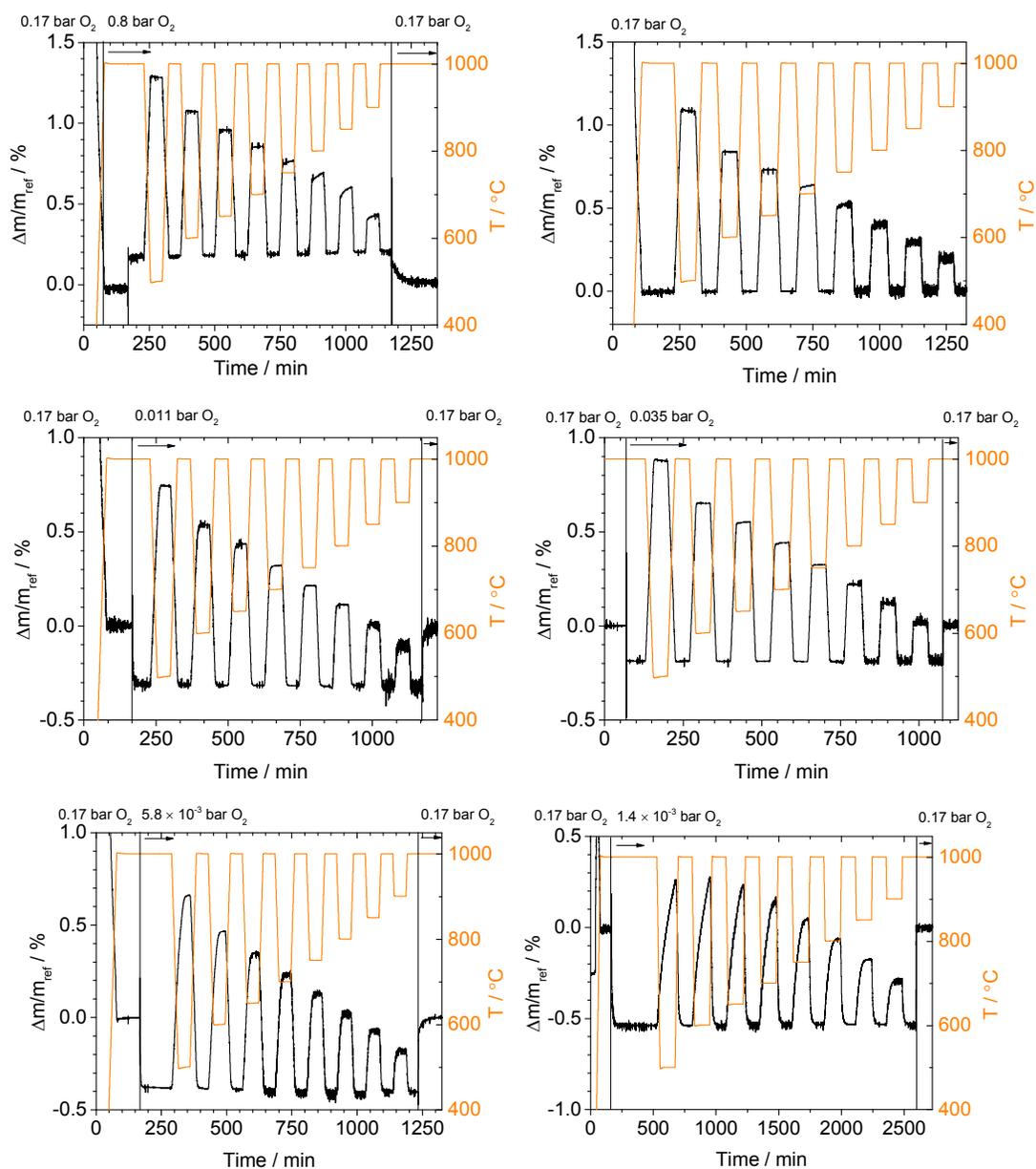
Figure S4. Buoyancy-corrected TGA profiles acquired from $SrCo_{0.9}Nb_{0.1}O_{3-\delta}$ under the following pO_2, listed clockwise from top left: 0.8, 0.17, 0.035, 1.4×10^{-3}, 5.8×10^{-3}, and 0.011 bar. At the beginning and end of each profile, the sample was exposed to 0.17 bar O_2 as indicated.
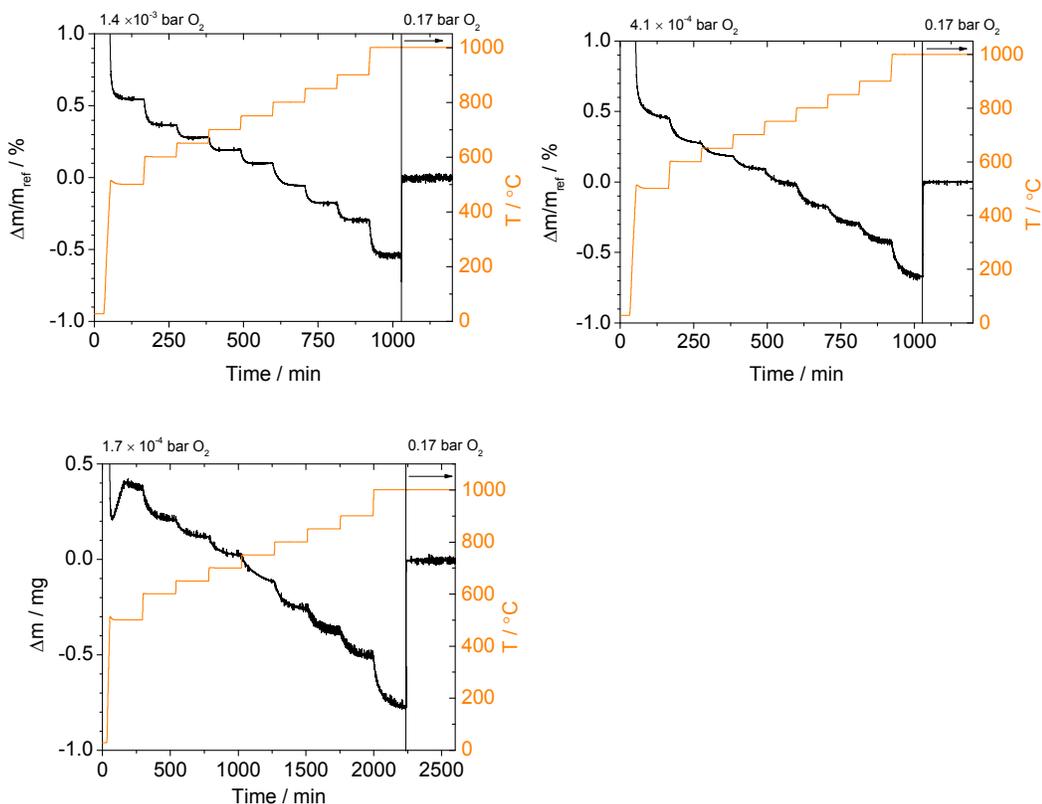
Figure S5. Buoyancy-corrected thermogravimetric profiles obtained at pO_2 of (clockwise from top left) 1.4×10^{-3}, 4.1×10^{-4}, and 1.7×10^{-4} bar O_2. An exponential decay function was fit to the mass profile at each temperature to determine the limiting mass value.
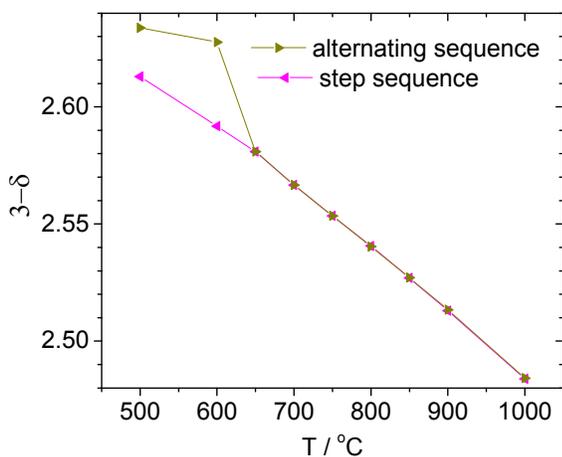
Figure S6. Comparison of implied oxygen stoichiometry in $SrCo_{0.9}Nb_{0.1}O_{3-\delta}$ from two different measurement protocols at $pO_2 = 1.4 \times 10^{-3}$ bar. (At 500 and 600 °C, the alternating sequence protocol did not provide sufficient time for equilibration, so at these two conditions only the step sequence data are considered reliable.)
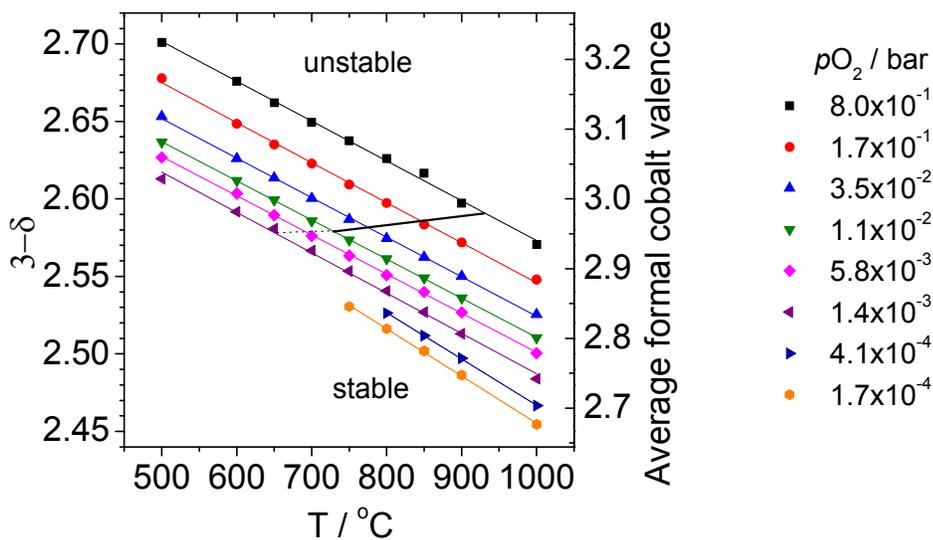
Figure S7. Oxygen stoichiometry 3-δ of $SrCo_{0.9}Nb_{0.1}O_{3-\delta}$. The nearly horizontal black line is based on Equation 1, the boundary between the thermodynamically stable and unstable regions as determined by the features of the thermogravimetric profiles. An extrapolated boundary is shown as a dashed line. Within the unstable region, the oxygen content represents the metastable behavior. Relative error bars at the 95% confidence level (not shown) were calculated to be ±0.020 at 1000 ℃ and ±0.014 or narrower at other temperatures. Solid lines are second-order polynomial fits. The corresponding average formal cobalt valence is also shown.
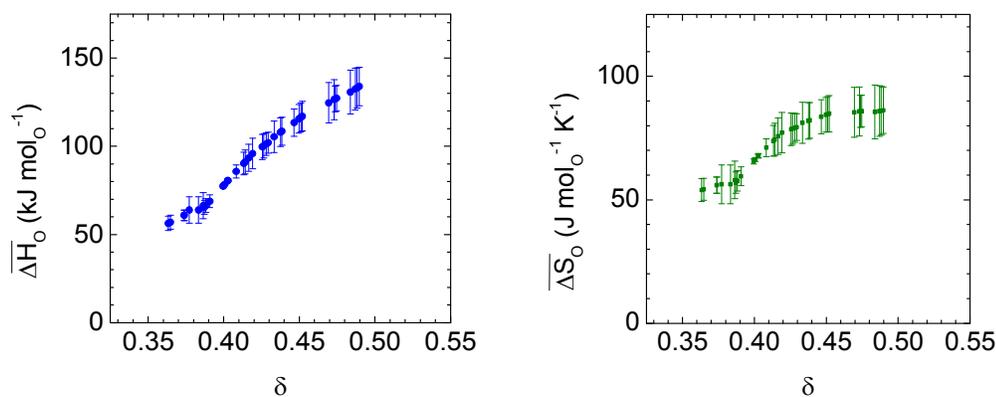
Figure S8. Relative partial molar enthalpy $\overline{\Delta H_O}$ and entropy $\overline{\Delta S_O}$ of oxygen in $SrCo_{0.9}Nb_{0.1}O_{3-\delta}$.
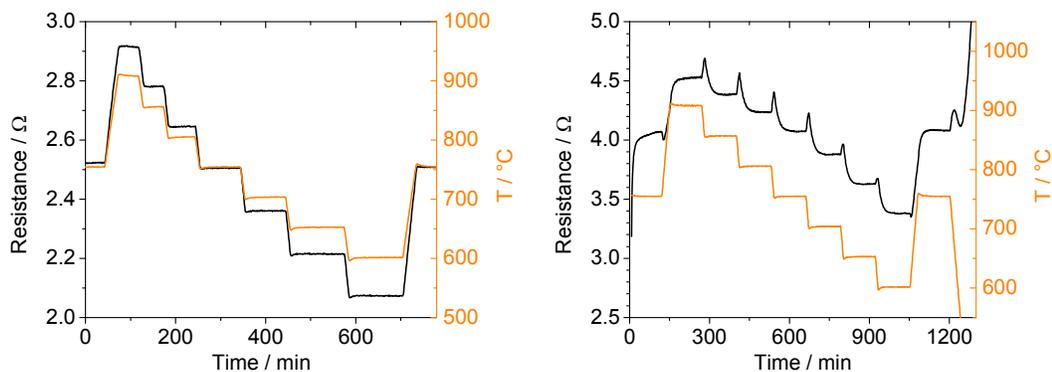
Figure S9. Raw resistance values measured from a sintered $SrCo_{0.9}Nb_{0.1}O_{3-\delta}$ compact at (a) 0.2 bar O_2 and (b) 1×10^{-4} bar O_2. The profiles in (a) are representative of all measurement atmospheres except that shown in (b). (The before-and-after verification at 700 °C was inadvertently omitted in the 1 bar O_2 condition, but was performed for all others.) The thermally activated transport behavior is also apparent in the unusual relaxation profile observed for conductivity measurements under low pO_2, at which oxidation kinetics are slow. At each temperature decrement of the profile, there is an initial *increase* in resistance, which is attributed to the thermally activated nature of the transport, followed by a subsequent *decrease* in resistance, which reflects slow isothermal oxygen uptake.

Discussion of electronic conductivity

The electronic conductivity of a species i that exhibits hopping behavior is described by the Nernst-Einstein relation:

$$\sigma_i = \frac{(z_i e)^2}{w_i k_B T} c_i D_i$$

where σ_i is electronic conductivity, z_i is valence, c_i is concentration, D_i is diffusivity, w_i is the thermodynamic factor, and k_B is the Boltzmann constant. [Maier, *Physical Chemistry of Ionic Materials*, p. 264] The diffusivity can be written as: [p. 284]

$$D_i = (1 - x_i)\gamma a_0^2 \frac{k_B \Theta_D}{h} \exp\left(\frac{-\Delta_m G}{k_B T}\right)$$

where x_i is the fraction of sites available to species i that are filled, γ is a constant (typically 1/6) that reflects the number of possible hopping directions, a_0 is the lattice parameter, Θ_D is the Debye temperature, h is the Planck constant, and $\Delta_m G$ is the Gibbs energy of hole migration. Combining these two relations,

$$\sigma_i = \frac{(z_i e)^2}{w_i k_B T} c_i (1 - x_i)\gamma a_0^2 \frac{k \Theta_D}{h} \exp\left(\frac{-\Delta_m G}{k_B T}\right)$$

or

$$\sigma_i = \frac{C}{T} \exp\left(\frac{-\Delta_m H}{k_B T}\right)$$

where the parameter C includes contributions from the concentration, the thermodynamic factor, and the entropy of hole migration $\Delta_m S$. The use of Θ_D in the transition state prefactor implicitly assumes that $T > \Theta_D$, which is reasonable here. The temperature dependence of the thermodynamic factor is assumed to be negligible relative to the exponential factor of interest here. Changes in the mobile carrier concentration with temperature at fixed δ due to disproportionation (*e.g.*, $2Co^{3+} \rightarrow Co^{2+} + Co^{4+}$) are neglected; the relatively small temperature range of the analysis limits the error associated with this approximation.
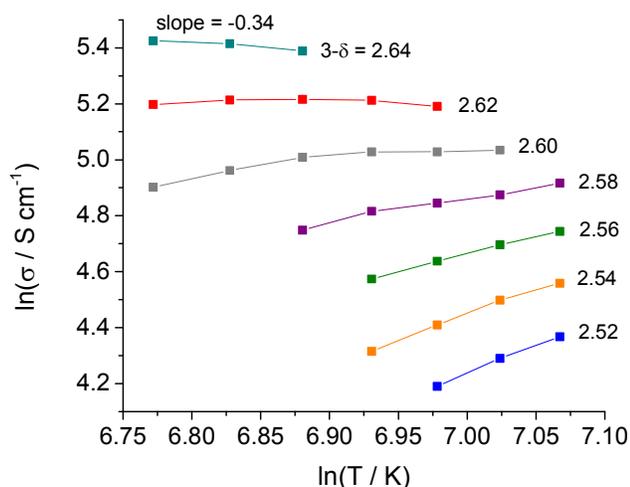
Figure S10. Iso-stoichiometric electronic conductivity of SCN as a function of temperature. At all but the highest oxygen content, the conductivity increases with temperature. As oxygen stoichiometry increases, the slope of conductivity with temperature decreases, consistent with the small polarons in SCN becoming larger (more delocalized). At the highest oxygen stoichiometry studied, the lowest observed slope is -0.34, not -1.0 as would be expected for phonon scattering in a metal above the Debye temperature. Thus, SCN at high oxygen stoichiometries is a large polaronic conductor and appears to be approaching metallic behavior.
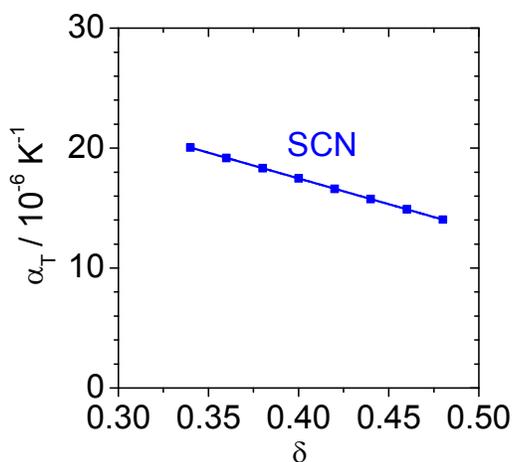
Figure S11. Thermal expansivity α_T of $SrCo_{0.9}Nb_{0.1}O_{3-\delta}$, shown with a linear fit.